Both nitric and hydrochloric acids also decompose the silicates and aluminates present in the cement matrix, thus confirming the fact that SE samples are more resistant to these acids since they contain less cement.

On the contrary, in the case of sulfuric acid the weight loss varies greatly if one considers the residual dust or not, and this means that the samples have been disintegrated but most of the powder formed is not dissolved in the solution. Sulfuric acid, when in contact with lime, forms gypsum; the formation of gypsum means that the weight loss is not as noticeable because the chemical nature of some elements has changed but these elements have not been dissolved in the acid.

3.4. SEM Analyses

SEM analyses were first performed on the pre attack SE samples, and the images obtained are reported in Figure 9.

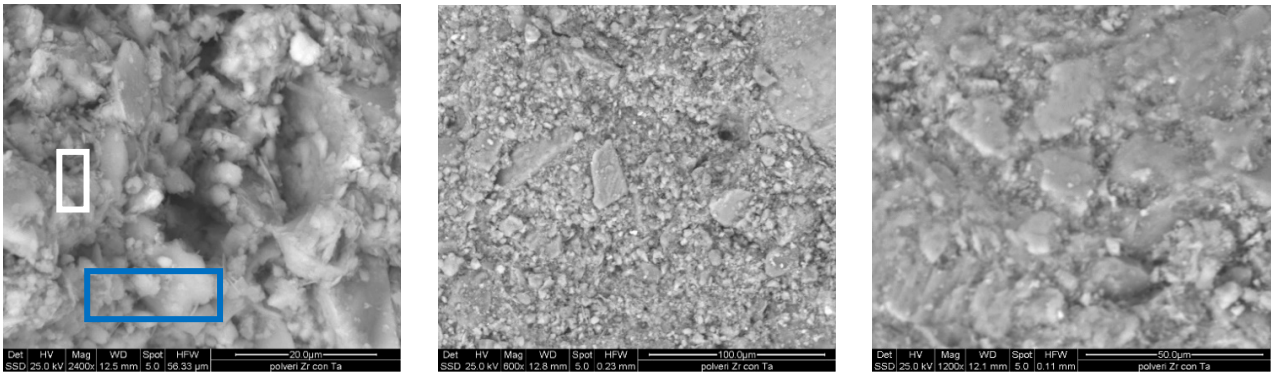

(**a**) (**b**) (**c**)

Figure 9. SEM images of pre attached SE samples. (**a**) (600×). (**b**) (1200×). (**c**) (2400×) Blue rectangles = gel area, White rectangle = aggregate.

The earth and cement fractions are well blended together as the binder matrix appears homogeneous. Some aggregates with dimensions between 10 and 20 µm are also distinguishable, and the interface between aggregate and matrix presents good adhesion.

In Figure 9a it is possible to see two highlighted areas. The blue area corresponds to cementitious gel with a chemical composition corresponding to Si = 20 wt% and Ca = 30%, determined by EDS analysis. The chemical composition of the aggregate (white area) shows a higher amount of silicon and a lower amount of Ca (Si = 28% and Ca = 7%), in agreement with siliceous aggregates. In the interface area intermediate chemical composition is observed, i.e. Si = 20% and Ca = 26% due to the chemical interaction between matrix and aggregate. The presence of the mentioned elements is shown in the EDS graphic of the blue area of the sample. In the post chloride attack of SE specimens, both inner and outer surfaces were analyzed, and the images are reported in Figure 10.

The samples appear to be fairly homogeneous both internally and externally, and no diffuse salt precipitation is observed. The main elements found in the examined samples are Silicon, Calcium, Aluminum, Magnesium, Chlorine, Iron, and Sodium. On the sample surface, the presence of chlorine is significant (about 6%), considering that it is only due to eluate residues, probably deposit is formed. Only in the outer surface samples, rare white dots are evident, with a chemical composition of Ca = 20% and Cl = 5%, corresponding to crystallization of calcium chlorides.

The chemical analysis of aggregate particles remains unchanged, corresponding to Si and O in agreement with their siliceous natures. From the chemical analysis of the inner part of the samples a significant concentration of chlorine is observed in the cementitious gel (Cl = 3.7–9wt%). From these data it seems that chlorine diffuses in the gel more than it concentrates in the crystals.

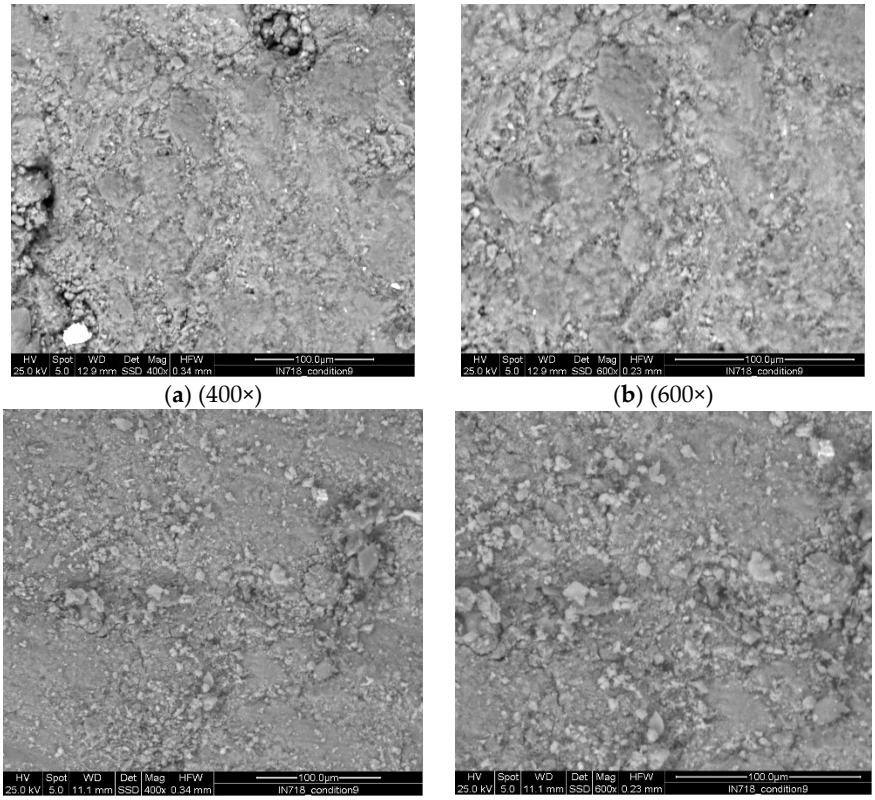

(**a**) (400×) (**b**) (600×)

(**c**) (400×) (**d**) (600×)

Figure 10. SEM images of outer surfaces (**a**,**b**) and inner (**c**,**d**) in SE sample post calcium chloride attack.

The presence of the Cl on the sample surface is also confirmed by the chemical analysis reported in Figure 11.

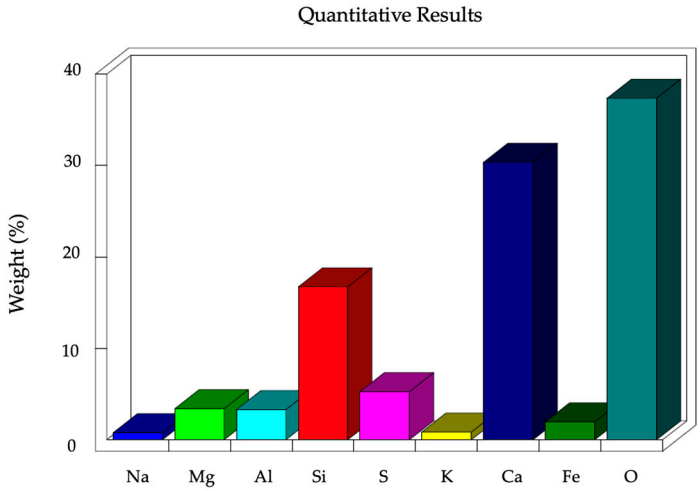

Figure 11. Semiquantitative chemical analysis of the outer surface of the SE sample after calcium chloride attack.

Regarding post attack samples from sodium sulfate, SEM images were taken from both the samples from the emerged side (thus where ettringite eventually forms, Figure 12a) and the immersed side (Figure 12b) and compared with the pre attack SE samples (Figure 9).

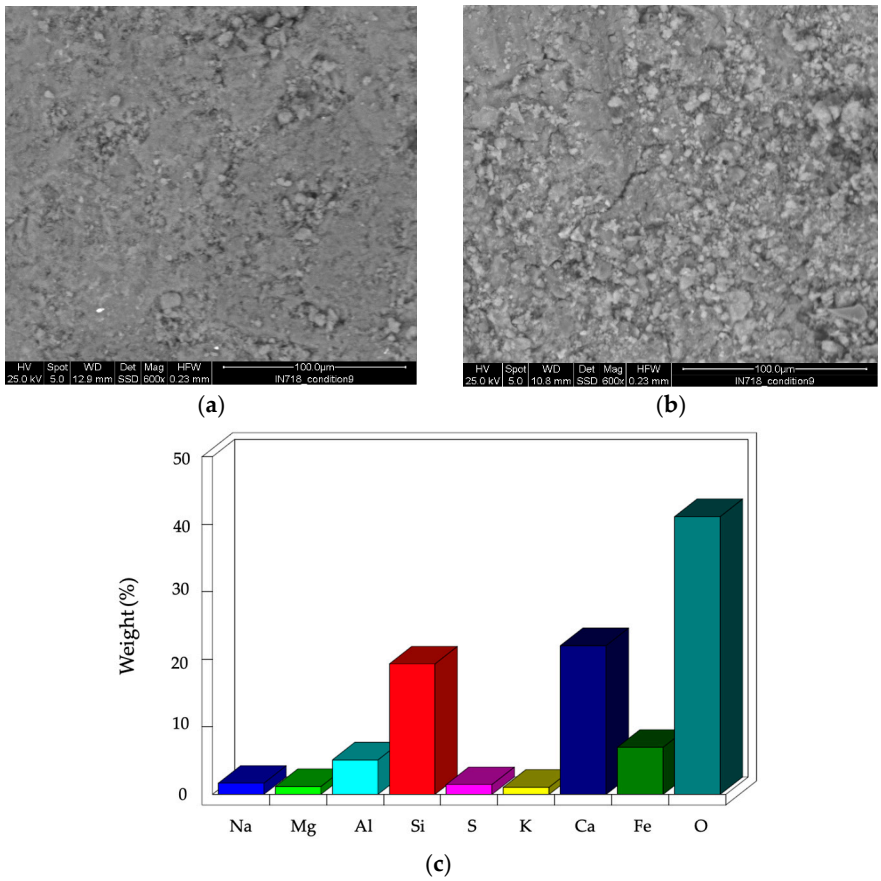

Figure 12. SEM images of the SE sample post sodium sulfate ((**a**) (600×)) emerged part and ((**b**) (600×)) immersed part. (**c**) Semiquantitative chemical analysis of emerged part.

It is worth noticing that no salts or fractures are evident from the images and the matrix appears to be homogeneous.

The elements present in the SE samples are mainly Calcium, Magnesium, Iron, Aluminum, Potassium, and Silicon (Figure 12). The percentages of these elements vary slightly, probably depending on the concentration of soil or the presence of aggregates, but since the soil and cement are perfectly amalgamated, it is impossible to state which elements relate to the soil alone and which to the cement.

Analyzing the immersed part makes it evident that Sulphur is homogenously distributed in the sample with a concentration of 1.1–1.95%, but it is particularly concentrated in the cementitious gel with an average concentration of 4 wt% (Figure 12).

Also, analysis of the sample corresponding to the surface content of Sulphur that is not immersed is also observed, and this probably can be related to diffusion of Sulphur inside the sample.

3.5. XRD Analyses

XRD analysis was carried out, for all types of samples, pre attack, after acid attack, after calcium chloride attack, and after sodium sulfate attack, to see the crystal structure of the samples and whether this changes after exposure to aggressive agents.

Comparisons were then made to see how the crystal structure changed in the different situations, i.e., in contact with calcium chloride and hydrochloric acid, sodium sulfate and sulfuric acid, and finally in contact with nitric acid.

- HCl and calcium chloride

The crystalline phases present in the SE pre attack samples are quartz coming from both aggregates, matrix, and calcite. After an attack by calcium chloride, a slight decrease in the peak related to calcite (29°) is seen, but the graphs remain about the same. After the attack by hydrochloric acid, on the other hand, the peak relating to calcite (29°) disappears, due to the high solubility of this phase in HCl, and quartz remains the only phase present (Figure 13a). This is because the calcium present in the form of calcium hydroxide reacts with hydrochloric acid to form calcium chloride, which is a very soluble substance, so only the quartz of the aggregates remains in the sample, which does not dissolve in contact with the acid.

In pre attack concrete and mortar (Figure 13b,c) samples, in addition to quartz and calcite, dolomite is also present. In both samples after attack by calcium chloride (Figure 13b,c), the peaks of the dolomite and calcite decrease in favor of quartz, although the crystalline phases do not change. After the attack of hydrochloric acid, the peaks for calcite and dolomite disappear in favor of a quartz increase, since calcium has reacted and turned into calcium chloride.

- H_2SO_4 and sodium sulfate

The pre and post attack XRD patterns from sodium sulfate appears to be quite similar for every sample, and only few small peaks related to calcite decrease for SE (Figure 14a), while for C (Figure 14b) and M (Figure 14c) samples the dolomite peak decreases significantly in favor of calcite.

On the contrary, with the acid attack, XRD patterns pre and post acid attack change significantly; calcium in the form of calcium hydroxide in contact with sulfuric acid forms gypsum, which in the case of the SE sample is present in an important way (peaks at 11°, 21°, 29°, 31°, 33°), going on to consume all the calcite whose peaks disappear. The peaks related to quartz, on the other hand, remain almost unchanged, since quartz does not react with the acid. Gypsum, quartz, and residual calcite or dolomite are the crystalline phases present post sulfuric acid attack.

- HNO_3

For nitric acid there is no comparison with the related salt, but it is interesting to see how the peaks related to calcite (and for the C and M samples also to dolomite) disappear due to their solubility and the free Ca formed reacts with the acid to form calcium nitrate. Quartz remains the only crystalline phase present after a nitric acid attack for all the samples (Figure 15).

In general, what can be said in relation to all the XRD patterns examined is that the samples behave consistently with each other, and those containing more aggregates (and therefore more quartz) are more resistant to attacks, especially acid attacks. SE samples turn out to be more resistant to attacks because, in addition to containing aggregates, they contain less calcium since part of the cement is replaced by soil, and this allows for less reactivity and consequently leads to a lower weight loss. These considerations are consistent for all the salts and the acids tested, except for nitric acid, where the weight loss turns out to be greater for SE than in the other samples tested.

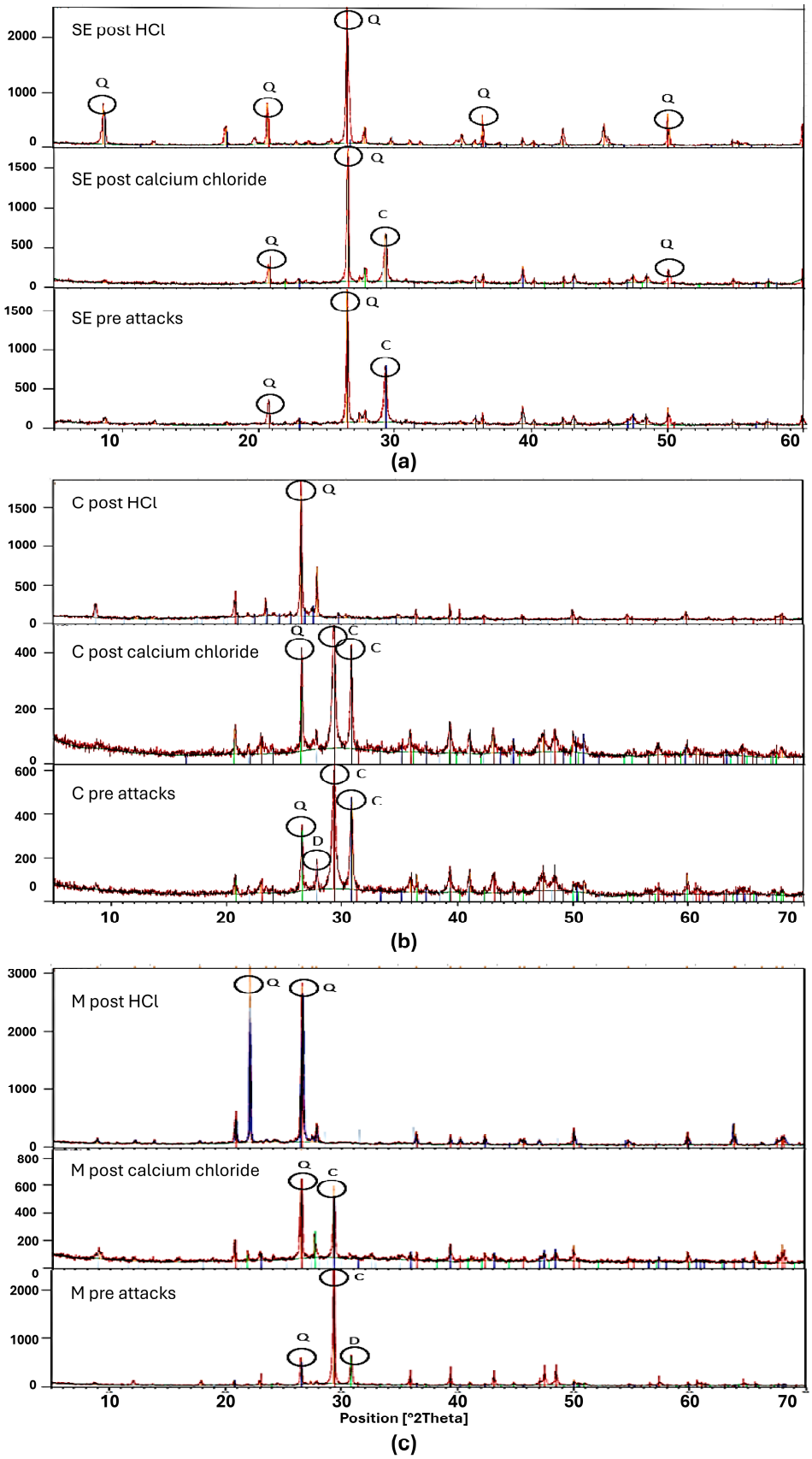

Figure 13. SE (**a**), C (**b**), and M (**c**) comparison pre attack, after calcium chloride, and post hydrochloric acid attack. (C = calcite, Q = quartz, D = dolomite).

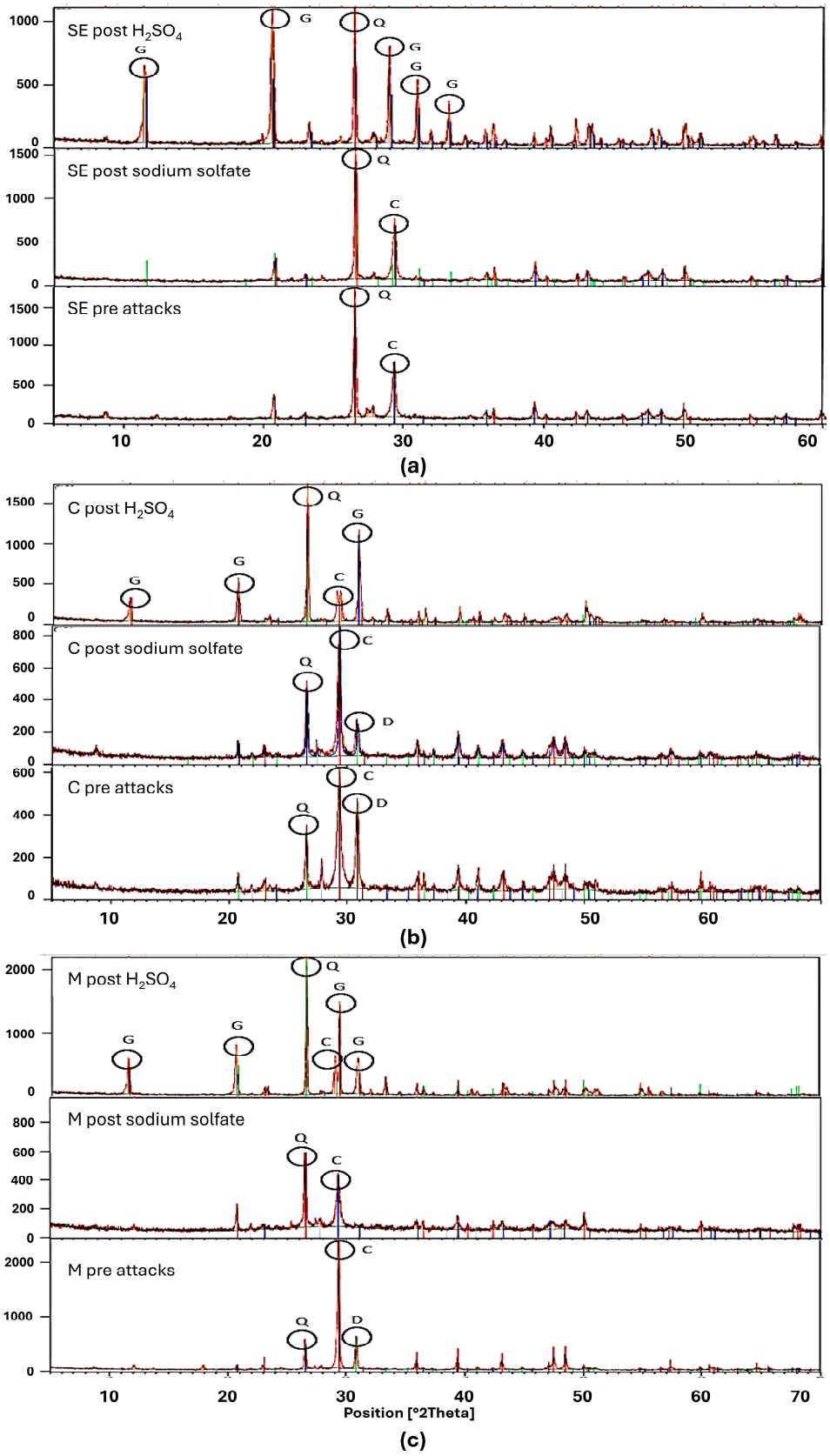

Figure 14. SE (**a**), C (**b**), and M (**c**) comparison pre attack, post sodium sulfate, and post sulfuric acid attack. (C = calcite, Q = quartz, D = dolomite, G = Gypsum).

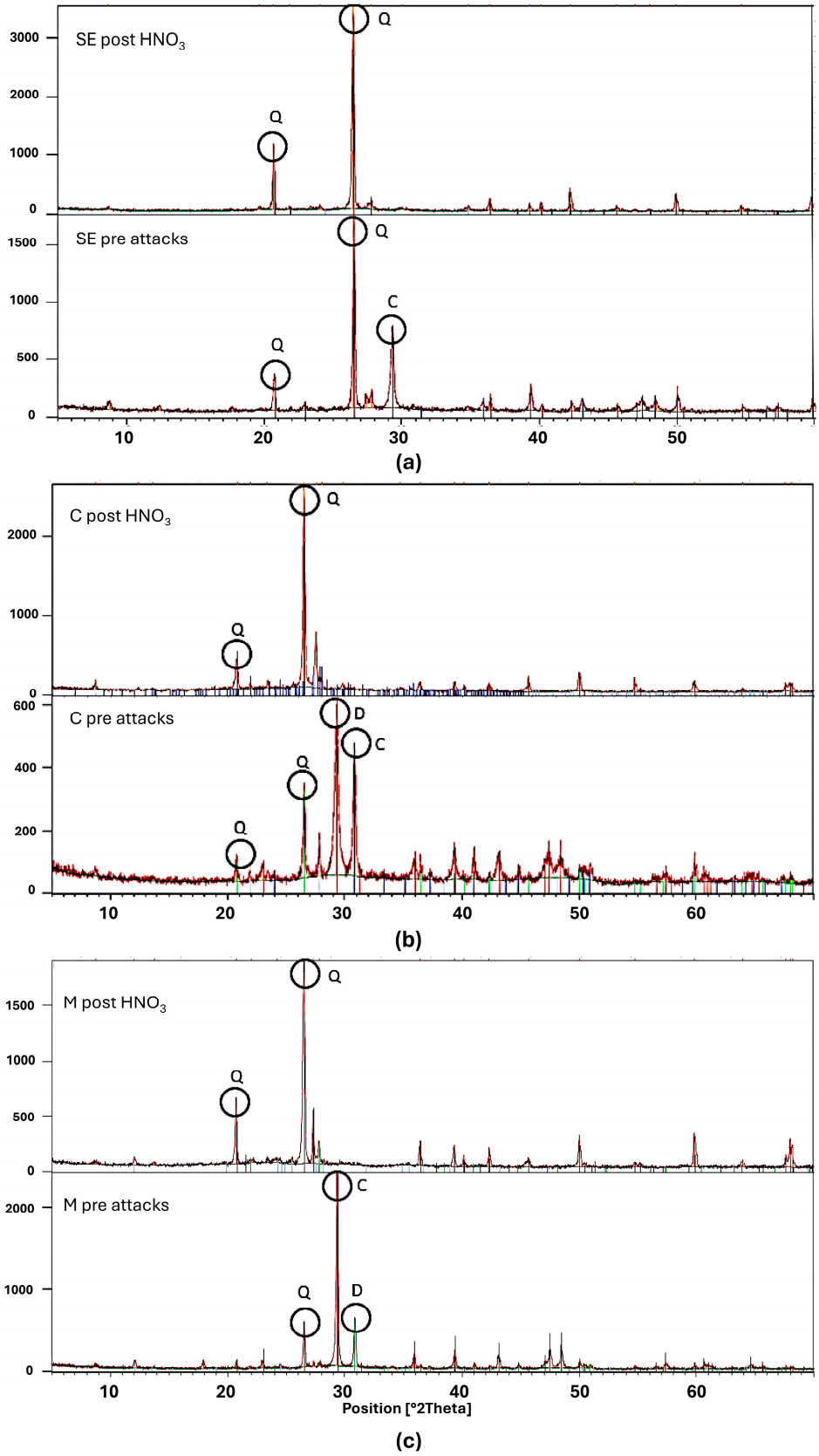

Figure 15. SE (**a**), C (**b**), and M (**c**) comparison before and after nitric acid attack. (C = calcite, Q = quartz, D = dolomite).

4. Conclusions

The main physical and chemical performances of SE samples have been identified through a comprehensive experimental campaign and compared to those exhibited by conventional cementitious composites like concrete and mortar. Summing up, this study carried out yields with positive implications. In detail, the values of the true density (2636 g/cm^3) and porosity (29%) confirm that the SE samples are in line with the reference ones. The same can be said for the capillary water absorption test, which places the SE samples in category W1 according to UNI EN 998-1:2010, the same category as mortar. Although mechanically weaker, SE specimens are generally more resistant to chemical attack by salts, precisely because of the presence of earth that replaces cement and does not react. The compressive strength remains almost constant after chemical attack, while for concrete, a dramatic decrease in this property is evident (25.5 MPa before and 4.6 MPa after the CaC_{l2} attack).

Even in acid attacks, the substitution of cement by earth plays an important role in the resistance of the samples to acid contact. In particular, the SE samples also showed greater resistance to nitric acid and hydrochloric acid than the reference samples, reporting a lower percentage of weight loss, 25% for hydrochloric acid and 45% for nitric acid. This is because the soil used in SE samples replaces part of the cement, resulting in less lime available to react. However, with sulfuric acid, there is a greater weight loss from SE samples compared to the reference ones, although it is still a relatively low value (21%). These results have been corroborated by XRD and SEM analyses, which allow for assessing the final conditions of the samples after acid attacks. The investigation confirms that the SE samples have good resistance to chemical attacks.

Therefore, given the results obtained in this study, it is possible to conclude that the durability of SE samples is perfectly in line with that of mortar and concrete, if not, in some cases, even better. The outcomes obtained in the present paper can be interpreted as a benchmark to corroborate further investigations about the durability of SE construction. Particularly, this study highlighted that the durability of SE and soil-based material must be assessed, taking into account specific chemical and physical aspects to avoid implementing durability-enhancing strategies at the mix design or technological level that are not needed nor effective. Finally, this study will permit the creation of further optimization strategies for construction in sustainable excavated soil leading to the use of less cement with a corresponding lower amount of CO_2 emitted for the clinker production.

Author Contributions: Conceptualization, L.B., I.L., L.L. and A.M.T.; methodology, L.B., I.L. and L.L.; investigation, R.M. and S.I.; data curation, I.L., L.L. and R.M.; writing—original draft preparation, L.B., I.L., L.L. and R.M.; writing—review and editing, L.B., I.L. and L.L.; supervision, L.B., I.L. and L.L.; project administration, L.L.; funding acquisition, L.L. All authors have read and agreed to the published version of the manuscript.

Funding: This research was funded by Authors gratefully acknowledge the financial support provided by HEIG-VD/HES-SO under the frame of the projects Terre 2020, Next Earth building and U-More earth. Financial support from the Italian Ministry of University and Research (MUR) in the framework of the Project FISA2022 "EARTH-TECH" (code 00183; CUP: E93C24000250001) is gratefully acknowledged. The authors are grateful to the firm *Pittet Artisans* sárl for their support in manufacturing the specimens and optimizing the Shot-earth mix. Finally, financial support from University of Modena and Reggio Emilia in the framework of "FAR Dipartimentale 2022-2023" (CUP: E93C22000590005) is gratefully acknowledged.

Institutional Review Board Statement: The study did not require ethical approval.

Informed Consent Statement: Not applicable.

Data Availability Statement: The data presented in this study are available on request from the corresponding author.

Conflicts of Interest: The authors declare no conflict of interest.

References

1. Hale, S.E.; Roque, A.J.; Okkenhaug, G.; Sørmo, E.; Lenoir, T.; Carlsson, C.; Kupryianchyk, D.; Flyhammar, P.; Žlender, B. The Reuse of Excavated Soils from Construction and Demolition Projects: Limitations and Possibilities. *Sustainability* **2021**, *13*, 6083. [CrossRef]
2. Tarantino, A.M.; Cotana, F.; Viviani, M. (Eds.) *Shot-Earth for an Eco-Friendly and Human-Comfortable Construction Industry*; Springer Tracts in Civil Engineering; Springer Nature: Cham, Switzerland, 2023; ISBN 978-3-031-23506-1.
3. Savino, V.; Franciosi, M.; Viviani, M. Engineering and Analyses of a Novel Catalan Vault. *Eng. Fail. Anal.* **2023**, *143*, 106841. [CrossRef]
4. Scrivener, K.; Martirena, F.; Bishnoi, S.; Maity, S. Calcined Clay Limestone Cements (LC3). *Cem. Concr. Res.* **2018**, *114*, 49–56. [CrossRef]
5. Bacciocchi, M.; Savino, V.; Lanzoni, L.; Tarantino, A.M.; Viviani, M. Multi-Phase Homogenization Procedure for Estimating the Mechanical Properties of Shot-Earth Materials. *Compos. Struct.* **2022**, *295*, 115799. [CrossRef]
6. Curto, A.; Lanzoni, L.; Tarantino, A.M.; Viviani, M. Shot-Earth for Sustainable Constructions. *Constr. Build. Mater.* **2020**, *239*, 117775. [CrossRef]
7. D'Alessandro, A.; Fabiani, C.; Pisello, A.L.; Ubertini, F.; Materazzi, A.L.; Cotana, F. Innovative Concretes for Low-Carbon Constructions: A Review. *Int. J. Low-Carbon Tech.* **2016**, *12*, 289–309. [CrossRef]
8. Elsvier Article: Shot-Earth for Sustainable Constructions. Available online: https://www.pittet-artisans.ch/blog/elsvier-article-shot-earth-for-sustainable-constructions.html (accessed on 12 January 2020).
9. Robalo, K.; Soldado, E.; Costa, H.; Carvalho, L.; Do Carmo, R.; Júlio, E. Durability and Time-Dependent Properties of Low-Cement Concrete. *Materials* **2020**, *13*, 3583. [CrossRef] [PubMed]
10. Soldado, E.; Antunes, A.; Costa, H.; Do Carmo, R.; Júlio, E. Durability of Mortar Matrices of Low-Cement Concrete with Specific Additions. *Constr. Build. Mater.* **2021**, *309*, 125060. [CrossRef]
11. Scherer, G.W. Stress from Crystallization of Salt. *Cem. Concr. Res.* **2004**, *34*, 1613–1624. [CrossRef]
12. Medina, G.; Sáez Del Bosque, I.F.; Frías, M.; Sánchez De Rojas, M.I.; Medina, C. Durability of New Recycled Granite Quarry Dust-Bearing Cements. *Constr. Build. Mater.* **2018**, *187*, 414–425. [CrossRef]
13. Tobón, J.I.; Payá, J.; Restrepo, O.J. Study of Durability of Portland Cement Mortars Blended with Silica Nanoparticles. *Constr. Build. Mater.* **2015**, *80*, 92–97. [CrossRef]
14. Vantadori, S.; Żak, A.; Sadowski, Ł.; Ronchei, C.; Scorza, D.; Zanichelli, A.; Viviani, M. Microstructural, Chemical and Physical Characterisation of the Shot-Earth 772. *Constr. Build. Mater.* **2022**, *341*, 127766. [CrossRef]
15. Colpo, A.; Vantadori, S.; Friedrich, L.; Zanichelli, A.; Ronchei, C.; Scorza, D.; Iturrioz, I. A Novel LDEM Formulation with Crack Frictional Sliding to Estimate Fracture and Flexural Behaviour of the Shot-Earth 772. *Compos. Struct.* **2023**, *305*, 116514. [CrossRef]
16. *UNI EN 1936:2006*; Test Methods for Natural Stones—Determination of Real and Apparent Density and Total and Open Porosity. UNI: Rome, Italy, 2006.
17. *UNI EN 1015-18:2004*; Test Methods for Masonry Mortars—Determination of the Capillarity Water Absorption Coefficient of the Hardened Mortar. UNI: Rome, Italy, 2004.
18. *UNI EN 998-2:2016*; Specifications for Masonry Mortars—Part 2: Masonry Mortars. UNI: Rome, Italy, 2016.
19. *EN 196-1:2005*; Methods of Testing Cement—Part 1: Determination of Strength. UNI: Rome, Italy, 2005.
20. *UNI-EN 206-1:2006*; Concrete—Part 1: Specification, Performance, Production and Conformity. UNI: Rome, Italy, 2006.
21. Danillo Wisky Silva, L.; Bufalino, M.A.; Martins, H.S.; Junior, G.; Tonoli, L. Mendes, Superabsorbent Ability Polymer to Reduce the Bulk Density of Extruded Cement Boards. *J. Build. Eng.* **2021**, *43*, 103130. [CrossRef]
22. Sadrmomtazi, A.; Noorollahi, Z.; Tahmouresi, B.; Saradar, A. Effects of Hauling Time on Self-Consolidating Mortars Containing Metakaolin and Natural Zeolite. *Constr. Build. Mater.* **2019**, *221*, 283–291. [CrossRef]
23. *UNI EN 998-1:2010*; Specification for mortar for masonry—Part 1: Rendering and plastering mortar. UNI: Rome, Italy, 2011.
24. Türkel, S.; Felekoğlu, B.; Dulluç, S. Influence of Various Acids on the Physico-Mechanical Properties of Pozzolanic Cement Mortars. *Sadhana* **2007**, *32*, 683–691. [CrossRef]
25. Chandra, S. Hydrochloric Acid Attack on Cement Mortar—An Analytical Study. *Cem. Concr. Res.* **1988**, *18*, 193–203. [CrossRef]
26. Pavlík, V. Corrosion of Hardened Cement Paste by Acetic and Nitric Acids Part II: Formation and Chemical Composition of the Corrosion Products Layer. *Cem. Concr. Res.* **1994**, *24*, 1495–1508. [CrossRef]
27. Sahoo, S.; Das, B.B.; Mustakim, S. Acid, Alkali, and Chloride Resistance of Concrete Composed of Low-Carbonated Fly Ash. *J. Mater. Civ. Eng.* **2017**, *29*, 04016242. [CrossRef]
28. Min, H.; Song, Z. Investigation on the Sulfuric Acid Corrosion Mechanism for Concrete in Soaking Environment. *Adv. Mater. Sci. Eng.* **2018**, *2018*, 3258123. [CrossRef]
29. Irico, S.; De Meyst, L.; Qvaeschning, D.; Alonso, M.C.; Villar, K.; De Belie, N. Severe Sulfuric Acid Attack on Self-Compacting Concrete with Granulometrically Optimized Blast-Furnace Slag-Comparison of Different Test Methods. *Materials* **2020**, *13*, 1431. [CrossRef] [PubMed]
30. Jankovic, K.; Milicic, L.; Stankovic, S.; SuSic, N. Investigation of the Mortar and Concrete Resistance in Aggressive Solutions. *Teh. Vjesn.* **2014**, *21*, 173–176.

31. Bin, T.; Cohen, M.D. Does Gypsum Formation during Sulfate Attack on Concrete Lead to Expansion? *Cement Concr. Res.* **2000**, *30*, 117–123.
32. Tian, B.; Cohen, M.D. Expansion of Alite Paste Caused by Gypsum Formation during Sulfate Attack. *J. Mater. Civ. Eng.* **2000**, *12*, 24–25. [CrossRef]